# A Study on Circular Disk Resonators on a Ferrite Substrate

KIYOMICHI ARAKI, DONG IL KIM, STUDENT MEMBER, IEEE, AND YOSHIYUKI NAITO, SENIOR MEMBER, IEEE

*Abstract*—**In this paper, an exact analysis of a circular disk resonator on a magnetized ferrite substrate which can be used for tunable filters and circular polarizing radiators is presented. The method makes use of Galerkin's method applied in the Hankel transform domain and is quite suitable for numerical calculation. The calculated values of the resonant frequencies and unloaded $Q$'s are shown to be in good agreement with the measured data and the validity of the present theory is confirmed.**

**Furthermore, the characteristics of the traveling wave filters are investigated theoretically and experimentally, and their advantages over the standing wave filters are demonstrated in terms of reflection and sensitivity of the $Q_L$ on the coupling strength.**

## I. Introduction

A CIRCULAR DISK conductor printed on a dielectric substrate backed by a ground plane is one of the fundamental components used in microwave integrated circuits and also can be operated as an antenna element for circular polarization in a printed antenna system. Although this component has been extensively investigated by microwave engineers and antenna engineers, most of these analyses are approximate treatments based on a modified cavity model. In such a model, a magnetic wall is assumed at the edge of the conductor and the radiation pattern is calculated from magnetic current flowing on this hypothetical magnetic wall [1], [2]. Because these resonators/radiators have two degenerate circulating modes, a careful treatment is required for exitation. Moreover, these resonant frequencies cannot be changed.

In this paper, a printed conductor on a magnetized ferrite substrate is studied thoroughly with a view to alleviating the above problems. In this proposed structure, the two modes will be nondegenerate owing to the anisotropy of magnetized ferrite and the resonant frequencies can be swept by changing the applied magnetic field. The analysis of these structures presented here is based on the Hankel transform domain approach [3], which has a number of attractive features: 1) unlike space domain approaches in terms of coupled integral equations, the spectral domain approach deals with simple algebraic equations; 2) no time-consuming inverse-transforms are needed to obtain the complex resonant frequency and the radiation pattern; 3) numerical processing is quite simple since we deal only with a small-size matrix eigenvalue problem because a certain physical nature of the unknown current on the disk can be incorporated in the formulation; and 4) the results for the complex resonant frequency are in a variational form. Numerical results for complex resonant frequencies are presented which are found to agree with measured data. Furthermore, the characteristics of traveling wave filters made of the new structure are investigated experimentally and their advantages over those of standing wave filters are demonstrated in terms of reflection and sensitivity of the loaded $Q$.

Manuscript received April 22, 1981; revised September 1, 1981.

The authors are with the Department of Electrical and Electronic Engineering, Tokyo Institute of Technology, Meguro-ku, Tokyo 152, Japan.

## II. Hankel Transform Domain Analysis

The structure under investigation is shown in Fig. 1, which is a circular disk conductor printed on a magnetized ferrite substrate backed by a ground plane. The dc magnetic field is applied in the $z$-direction perpendicular to the ground plane. The method of analysis presented here is based on the Galerkin's method applied in the Hankel transform domain [3].

### A. General Field Expressions in Magnetized Ferrites

To get general exact expressions for electromagnetic fields for a magnetized substrate, the conditions that $\partial/\partial z \neq 0$ and $H_z \neq 0$ are needed. Then Maxwell's equations can be arranged into the following form:

$$\nabla_t \times \mathbb{E}_t = -j\omega\mu_z \mathbb{H}_z \tag{1}$$

$$\nabla_t \cdot \mathbb{E}_t = -\frac{\partial}{\partial z} E_z = j\beta E_z \tag{2}$$

$$\nabla_t \times \mathbb{H}_t = j\omega\epsilon \mathbb{E}_z \tag{3}$$

$$\nabla_t \cdot \mathbb{H}_t = -\omega\epsilon\sigma E_z - \frac{\mu_z}{\mu}\frac{\partial}{\partial z} H_z = -\omega\epsilon\sigma E_z + j\beta\frac{\mu_z}{\mu} H_z \tag{4}$$

where $\partial/\partial z = -j\beta$ is assumed and the time factor $\exp(j\omega t)$ is omitted throughout, and the magnetized ferrite has the tensor permeability as follows:

$$[\mu] = \begin{bmatrix} \mu & -j\kappa & 0 \\ j\kappa & \mu & 0 \\ 0 & 0 & \mu_z \end{bmatrix} = \begin{bmatrix} 1 & -j\sigma & 0 \\ j\sigma & 1 & 0 \\ 0 & 0 & \mu_z/\mu \end{bmatrix} \mu. \tag{5}$$

From the above equations coupled differential equations governing $E_z$ and $H_z$ are derived

$$(\nabla_t^2 - \beta^2 + \omega^2\mu_e\epsilon) E_z = -j\omega\mu_z\sigma\beta H_z \tag{6}$$

0018-9480/82/0200-0147$00.75 ©1982 IEEE

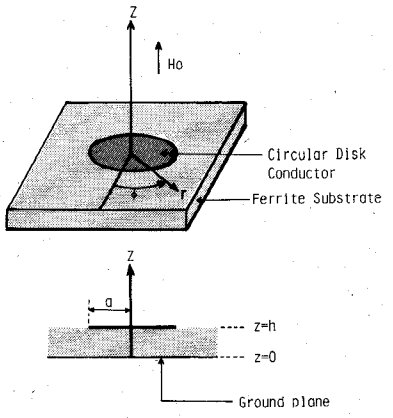


Fig. 1. A structure of circular disk resonator and the coordinate system adopted.

and

$$\left(\nabla_t^2 - \beta^2\frac{\mu_z}{\mu} + \omega^2\mu_z\epsilon\right)H_z = j\omega\epsilon\sigma\beta E_z \tag{7}$$

where $\mu_e = (\mu^2 - \kappa^2)/\mu$. Now $E_z$ and $H_z$ are written in the following forms:

$$\begin{Bmatrix} E_z \\ H_z \end{Bmatrix} e^{jn\phi}\int_0^\infty \begin{Bmatrix} \tilde{E}_z \\ \tilde{H}_z \end{Bmatrix} e^{-j\beta z} J_n(\alpha r)\alpha\, d\alpha \tag{8}$$

where $\tilde{E}_z$ and $\tilde{H}_z$ are functions of $\alpha$ and called Hankel transforms of $E_z$ and $H_z$. Then the equations (6) and (7) can be rewritten as follows:

$$\left(\alpha^2 + \beta^2 - \omega^2\mu_e\epsilon\right)\tilde{E}_z = j\omega\mu_z\sigma\beta\tilde{H}_z \tag{6'}$$

$$\left(\alpha^2 + \beta^2\frac{\mu_z}{\mu} - \omega^2\mu_z\epsilon\right)\tilde{H}_z = -j\omega\epsilon\sigma\beta\tilde{E}_z. \tag{7'}$$

Substituting (7') into (6'), $\beta$ will be obtained as a function of the wavenumber $\alpha$ in the $r$-direction

$$\beta_{1\atop 2} = \sqrt{\omega^2\epsilon\mu - \frac{\alpha^2}{2}\left(1+\frac{\mu}{\mu_z}\right) \pm \sqrt{\frac{\alpha^4}{4}\left(1-\frac{\mu}{\mu_z}\right)^2 + \omega^4\epsilon^2\kappa^2 - \omega^2\epsilon\alpha^2\kappa^2/\mu_z}}\,. \tag{9}$$

Finally, the general field expressions in the magnetized ferrite are given as follows:

$$\begin{Bmatrix} E_z \\ H_z \end{Bmatrix} = e^{jn\phi}\int_0^\infty \left[ \begin{Bmatrix} \tilde{E}_z^+ \\ -j\bar{Y}\tilde{E}_z^+ \end{Bmatrix} e^{-j\beta_1 z} + \begin{Bmatrix} \tilde{E}_z^- \\ j\bar{Y}\tilde{E}_z^- \end{Bmatrix} e^{j\beta_1 z} + \begin{Bmatrix} j\bar{Z}\tilde{H}_z^+ \\ \tilde{H}_z^+ \end{Bmatrix} e^{-j\beta_2 z} \right] Jn(\alpha r)\alpha\, d\alpha \tag{10}$$

where

$$\bar{Y} = \beta_1\omega\epsilon\sigma/\left(\alpha^2 + \beta_1^2\frac{\mu_z}{\mu} - \omega^2\epsilon\mu_z\right) \tag{11}$$

$$\bar{Z} = \beta_2\omega\mu_z\sigma/\left(\alpha^2 + \beta_2^2 - \omega^2\epsilon\mu_e\right). \tag{12}$$

When $\sigma = 0$, we have $\bar{Z} = \bar{Y} = 0$ then the fields can be decomposed into TM and TE waves.

### *B. Matrix Green's Function in the Hankel Transform Domain*

From the boundary conditions of the circular disk conductor structure, we can obtain the admittance (or impedance) matrix relating the transformed current on the conductor with the transformed electric field. As the ground plane is placed at $z = 0$ as shown in Fig. 1, it is readily shown by (1) and (2) that $H_z = 0$ and $(\partial/\partial z)E_z = 0$ at $z = 0$. From these conditions, we can get the relations as follows:

$$\tilde{E}_z^+ = \tilde{E}_z^- \qquad \tilde{H}_z^+ = -\tilde{H}_z^-\,. \tag{13}$$

Thus, substituting (13) into (10) we obtain the field distributions in the ferrite region $(0 < z < h)$ as follows:

$$\begin{Bmatrix} E_z \\ H_z \end{Bmatrix} = e^{jn\phi}\int_0^\infty \left[ \tilde{E}_z \begin{Bmatrix} \cos\beta_1 z \\ -\bar{Y}\sin\beta_1 z \end{Bmatrix} + \tilde{H}_Z \begin{Bmatrix} \bar{Z}\cos\beta_2 z \\ -\sin\beta_2 z \end{Bmatrix} \right] J_n(\alpha r)\alpha\, d\alpha \tag{14}$$

where $\tilde{E}_z$ and $\tilde{H}_z$ are unknown functions of $\alpha$ to be determined later. On the other hand, in the air region $(z > h)$, the propagation constant $\beta'$ is given by (15)

$$\beta' = \sqrt{\omega^2\mu_0\epsilon_0 - \alpha^2}\,. \tag{15}$$

The field distributions in the air region is given by

$$\begin{Bmatrix} E_z \\ H_z \end{Bmatrix} = e^{jn\phi}\int_0^\infty \begin{Bmatrix} \tilde{e}_z \\ \tilde{h}_z \end{Bmatrix} e^{-j\beta'(z-h)} J_n(\alpha r)\alpha\, d\alpha. \tag{16}$$

At the interface of the two regions $(z = h)$, $\mathbb{E}_t$ is continuous and, hence, $\nabla_t \times \mathbb{E}_t$ and $\nabla_t \cdot \mathbb{E}_t$ also become continuous. Thus, the following equations are easily derived from these conditions:

$$-j\omega\mu_0\tilde{h}_z = j\omega\mu_z\left(\bar{Y}\tilde{E}_z\sin\beta_1 h + \tilde{H}_z\sin\beta_2 h\right) \equiv \tilde{E}_e \tag{17}$$

$$j\beta'\tilde{e}_z = \beta_1\tilde{E}_z\sin\beta_1 h + \beta_2\bar{Z}\tilde{H}_z\sin\beta_2 h \equiv \tilde{E}_0. \tag{18}$$

On the other hand, there is a jump in $\mathbb{H}_t$ due to $\mathbb{J}_t$

$$(\nabla_t \times \mathbb{J}_t)_z = \nabla_t \cdot \mathbb{H}_t\Big|_{z=h-0}^{z=h+0} \tag{19}$$

$$\nabla_t \cdot \mathbb{J}_t = -(\nabla_t \times \mathbb{H}_t)\Big|_{z=h-0}^{z=h+0}. \tag{20}$$

In this case, if we express the current density $\mathbb{J}_t$ in $\mathbb{J}_t = (J_r, J_\phi)$, $J_\pm$ can be given as follows:

$$J_\pm = J_r \pm jJ_\phi. \tag{21}$$

The left-hand sides of (19) and (20) become

$$(\nabla_t \times \mathbb{J}_t)_z = e^{jn\phi}\int_0^\infty \tilde{J}_e J_n(\alpha r)\alpha\, d\alpha \tag{22}$$

where

$$\tilde{J}_e \equiv (\tilde{J}_+ + \tilde{J}_-)\alpha/2j \tag{23}$$

and

$$\nabla_t \cdot \mathbb{J}_t = e^{jn\phi}\int_0^\infty \tilde{J}_o J_n(\alpha r)\alpha\, d\alpha \tag{24}$$

where

$$\tilde{J}_0 \equiv (\tilde{J}_+ - \tilde{J}_-)\alpha/2. \tag{25}$$

Substituting the boundary conditions and (22) and (24) into (19) and (20) gives

$$\tilde{J}_e = j\beta'\tilde{h}_z + \omega\epsilon\sigma\{\tilde{E}_z\cos\beta_1 h + \bar{Z}\tilde{H}_z\cos\beta_2 h\} - \frac{\mu_z}{\mu}\{\beta_1\bar{Y}\tilde{E}_z\cos\beta_1 h + \beta_2\tilde{H}_z\cos\beta_2 h\} \tag{26}$$

$$\tilde{J}_0 = j\omega\epsilon\{\tilde{E}_z\cos\beta_1 h + \bar{Z}\tilde{H}_z\cos\beta_2 h\} - j\omega\epsilon_0\tilde{e}_z. \tag{27}$$

These equations derived above can be written in a more concise form by substituting (17) and (18), and rearranging the results as follows:

$$\begin{bmatrix}\tilde{J}_e\\ \tilde{J}_0\end{bmatrix} = \begin{bmatrix}Y_{ee} & Y_{e0}\\ Y_{0e} & Y_{00}\end{bmatrix}\begin{bmatrix}\tilde{E}_e\\ E_0\end{bmatrix} \tag{28}$$

where

$$Y_{ee} = -\beta'/\omega\mu_0 + \left[\left(\omega\epsilon\sigma - \frac{\mu_z}{\mu}\beta_1\bar{Y}\right)\frac{j\beta_2\bar{Z}}{\omega\mu_z}\cot\beta_1 h - \left(\omega\epsilon\sigma\bar{Z} - \frac{\mu_z}{\mu}\beta_2\right)\frac{j\beta_1}{\omega\mu_z}\cot\beta_2 h\right]/(\beta_1 - \beta_2\bar{Y}\bar{Z}) \tag{29a}$$

$$Y_{e0} = \left[\left(\omega\epsilon\sigma - \frac{\mu_z}{\mu}\beta_1\bar{Y}\right)\cot\beta_1 h - \left(\omega\epsilon\sigma\bar{Z} - \frac{\mu_z}{\mu}\beta_2\right)\bar{Y}\cot\beta_z h\right]/(\beta_1 - \beta_2\bar{Y}\bar{Z}) \tag{29b}$$

$$Y_{0e} = \frac{\epsilon}{\mu_Z}\bar{Z}(\beta_1\cot\beta_2 h - \beta_z\cot\beta_1 h)/(\beta_1 - \beta_2\bar{Y}\bar{Z}) \tag{29c}$$

$$Y_{00} = -\omega\epsilon_0/\beta' + j\omega\epsilon(\cot\beta_1 h - \bar{Y}\bar{Z}\cot\beta_z h)/(\beta_1 - \beta_2\bar{Y}\bar{Z}). \tag{29d}$$

Now we define $\tilde{E}_e$ and $\tilde{E}_0$ in the same manner as (23) and (25)

$$\tilde{E}_e = (\tilde{E}_+ + \tilde{E}_-)\alpha/2j \tag{30}$$

and

$$\tilde{E}_0 = (\tilde{E}_+ - \tilde{E}_-)\alpha/2. \tag{31}$$

Substituting (30) and (31) into (28), we obtain the admittance matrix relating the transformed current with the transformed electric field

$$\begin{bmatrix}\tilde{J}_+\\ \tilde{J}_-\end{bmatrix} = \begin{bmatrix}Y_{++} & Y_{+-}\\ Y_{-+} & Y_{--}\end{bmatrix}\begin{bmatrix}\tilde{E}_+\\ \tilde{E}_-\end{bmatrix} \tag{32}$$

where

$$Y_{++} = [Y_{ee} + Y_{00} + j(Y_{e0} - Y_{0e})]/2 \tag{33a}$$

$$Y_{+-} = [Y_{ee} - Y_{00} - j(Y_{e0} + Y_{0e})]/2 \tag{33b}$$

$$Y_{-+} = [Y_{ee} - Y_{00} + j(Y_{e0} + Y_{0e})]/2 \tag{33c}$$

$$Y_{--} = [Y_{ee} + Y_{00} - j(Y_{e0} - Y_{0e})]/2. \tag{33d}$$

The impedance matrix can be obtained by inverting (32).

$$\begin{bmatrix}\tilde{E}_+\\ \tilde{E}_-\end{bmatrix} = \begin{bmatrix}Z_{++} & Z_{+-}\\ Z_{-+} & Z_{--}\end{bmatrix}\begin{bmatrix}\tilde{J}_+\\ \tilde{J}_-\end{bmatrix} = \begin{bmatrix}Y_{++} & Y_{+-}\\ Y_{-+} & Y_{--}\end{bmatrix}^{-1}\begin{bmatrix}\tilde{J}_+\\ \tilde{J}_-\end{bmatrix}. \tag{34}$$

The impedance matrix given above can be thought of as a matrix of Green's function for the structure shown in Fig. 1.

### *C. Characteristic Equation for the Natural Resonant Frequency by Galerkin's Method*

In this section, the boundary condition on the metal disk is used to obtain the characteristic equation for the complex resonant frequencies. To this end, we expand the unknown current distributions on the disk conductor as

$$\tilde{J}_+ = \sum_{j=1}^{N} a_j\tilde{J}_{rj}^+ + j\sum_{j=1}^{M} b_j\tilde{J}_{\phi j}^+ \tag{35}$$

and

$$\tilde{J}_- = \sum_{j=1}^{N} a_j\tilde{J}_{rj}^- - j\sum_{j=1}^{M} b_j\tilde{J}_{\phi j}^- \tag{36}$$

where $\tilde{J}_{rj}$ and $\tilde{J}_{\theta j}$ are the known basis functions, and $a_j$ and $b_j$ are expansion coefficients to be determined.

We substitute (35) and (36) into (34) and take inner products of the resulting equations with all of $\tilde{J}_i^{\pm}$'s. The right-hand sides become zero by virtue of Parseval's relation

$$\int_0^\infty \tilde{J}_i^{\pm}\tilde{E}^{\pm}\alpha\, d\alpha = \int_0^\infty J_i^{\pm}\cdot E^{\pm} r\, dr = 0. \tag{37}$$

This is because the boundary conditions at $z = h$ are

$$J_j^{\pm} = 0 \qquad (r > a)$$

$$E^{\pm} = 0 \qquad (r \leq a).$$

To avoid divergence of integrals appearing in the characteristic equation, suitable combinations are chosen as follows:

$$\int_0^\infty \{\tilde{J}_{ri}^+\tilde{E}^+ + \tilde{J}_{ri}^-\tilde{E}^-\}\alpha\, d\alpha = 0 \tag{38}$$

$$\int_0^\infty \{\tilde{J}_{\phi i}^+\tilde{E}^+ - \tilde{J}_{\phi i}^-\tilde{E}^-\}\alpha\, d\alpha = 0. \tag{39}$$

The above equations may be rewritten in a matrix form

$$[P][A] = \begin{bmatrix}P_{++ij} & P_{+-ij}\\ P_{-+ij} & P_{--ij}\end{bmatrix}\begin{bmatrix}a_j\\ jb_j\end{bmatrix} = 0 \tag{40}$$

where

$$\begin{Bmatrix} P_{++ij} \\ P_{+-ij} \\ P_{-+ij} \\ P_{--ij} \end{Bmatrix} = \int_0^\infty \left\{ Z_{++} \begin{bmatrix} \tilde{J}_{ri}^{+} & \tilde{J}_{rj}^{+} \\ \tilde{J}_{ri}^{+} & \tilde{J}_{\phi j}^{+} \\ \tilde{J}_{\phi i}^{+} & \tilde{J}_{rj}^{+} \\ \tilde{J}_{\phi i}^{+} & \tilde{J}_{\phi j}^{+} \end{bmatrix} Z_{+-} \begin{bmatrix} \tilde{J}_{ri}^{+} & J_{rj}^{-} \\ -\tilde{J}_{ri}^{+} & \tilde{J}_{\phi j}^{-} \\ \tilde{J}_{\phi i}^{+} & \tilde{J}_{rj}^{-} \\ -\tilde{J}_{\phi i}^{+} & \tilde{J}_{\phi j}^{-} \end{bmatrix} \right.$$

$$\left. + Z_{-+} \begin{bmatrix} \tilde{J}_{ri}^{-} & \tilde{J}_{rj}^{+} \\ \tilde{J}_{ri}^{-} & \tilde{J}_{\phi j}^{+} \\ -\tilde{J}_{\phi i}^{-} & \tilde{J}_{rj}^{+} \\ -\tilde{J}_{\phi i}^{-} & \tilde{J}_{\phi j}^{+} \end{bmatrix} + Z_{--} \begin{bmatrix} \tilde{J}_{ri}^{-} & \tilde{J}_{rj}^{-} \\ -\tilde{J}_{ri}^{-} & \tilde{J}_{\phi j}^{-} \\ -\tilde{J}_{\phi i}^{-} & \tilde{J}_{rj}^{-} \\ \tilde{J}_{\phi i}^{-} & \tilde{J}_{\phi j}^{-} \end{bmatrix} \right\} \alpha \, d\alpha. \quad (41)$$

From (40), the determinant of $[p]$ must vanish for a nontrivial solution to exist. Therefore, the characteristic equation can be given by

$$f(\omega) = \det[p] = 0 \quad (42)$$

where $\omega$ is the natural resonant frequency of the circular disk resonator with magnetized ferrite substrate backed by the ground plane. The solution of this equation has a stationary nature because Galerkin's method has been used. In general, the real part of $\omega$ corresponds to resonant frequency, whereas the imaginary part of $\omega$ is a damping factor due to radiation phenomena.

## III. Numerical and Experimental Results

### A. Numerical Results

We take 2 basis functions for each current component as shown in Appendix I and employ two formulas for tensor permeability of ferrite shown in Appendix II to calculate the resonant frequencies, one for the saturated case, and the other for partially magnetized case. Semi-infinite integrals in the matrix $[P]$ are truncated at $\alpha = 50$ for most cases and Simpson's formula is used for numerical integrations.

We report here some numerical results on resonant frequencies and unloaded $Q$ factors when the loss is only by radiation. In Figs. 2, 3, and 4, the results of this theory are compared with those by the simple cavity approximation model as well as experimental data.

The resonant frequencies computed by the full-wave analysis (Hankel transform domain approach) agree with the experimental data quite well, because all effects associated with radiation and leakage are taken into account in this method, whereas the results based on the cavity approximation are too high. This is conjectured to be caused by the fact that the field leakage is not considered in the cavity model in which the hypothetical magnetic wall is assumed at the edge of the disk conductor.

Next, let us discuss the unloaded $Q$ factors. When the external dc magnetic field is applied, a pair of degenerate modes splits into clockwise and counter-clockwise modes. If the dc field is applied in the direction in which $\kappa$ has a negative value, the clockwise mode's energy will be stored more in the inner side of the resonator than in the counter-clockwise case. Thus the radiation loss is relatively small in the case where $\kappa$ has a negative sign.

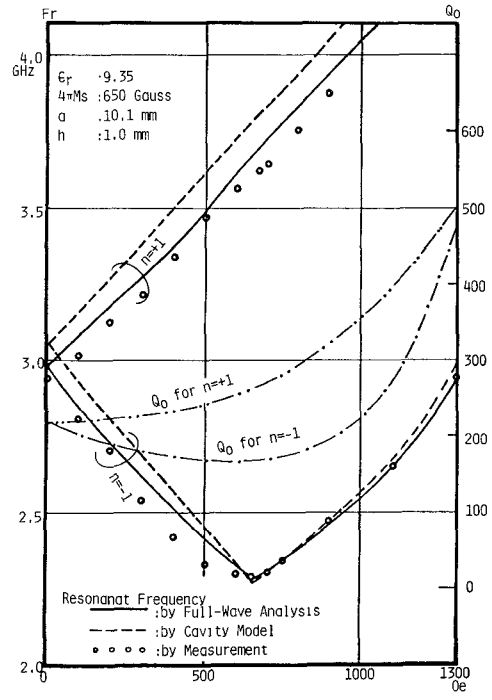


Fig. 2. Comparison with the experimental and calculated results by the full-wave analysis (including $Q_0$) along with a cavity model.

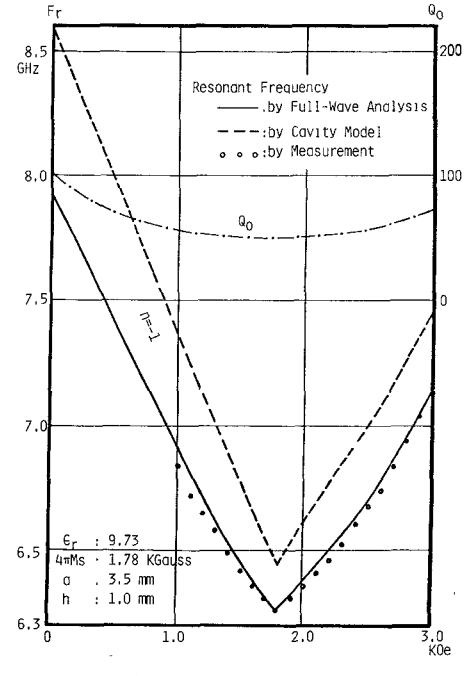


Fig. 3. Comparison with the experimental and calculated results by the full-wave analysis (including $Q_0$) along with a cavity model.

### B. Experimental Results

*1) Resonant Frequency:* First, we performed the experiments to examine whether or not the resonant frequencies calculated by the full-wave analysis in Section II agree well

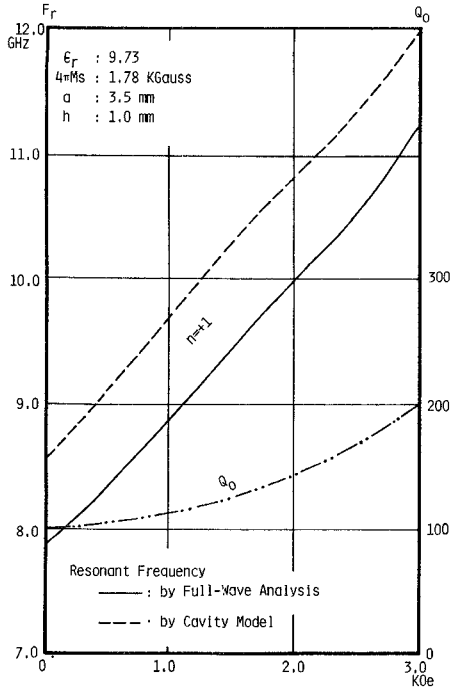


Fig. 4. Comparison of the calculated results by the full-wave analysis (including $Q_0$) and those by a cavity model.

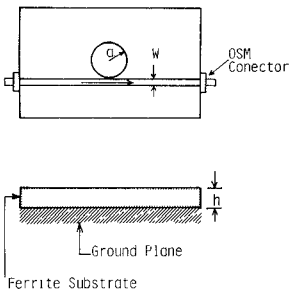


Fig. 5. A figure of the samples used in experiments.

with measured data. Fig. 5 shows the structure used in our experiments. The ferrite material has the saturation magnetization $4\pi M_s = 650$ G. The dimensions of the structure are as follows: ferrite thickness $h = 1.0$ mm, radius of circular disk $a = 10.1$ mm.

It was shown that the resonant frequencies by the full-wave analysis agreed with the experimental values very well as illustrated in Fig. 2. Next the measured resonant frequencies for $4\pi M_s = 1780$ G are compared with the calculated values in Figs. 3 and 4. Our results agree also with the measured values better than those by the cavity model. In Fig. 2, we can see that the resonant frequencies calculated by the cavity model also agree with the measured values favorably as long as $h/a$ is small, i.e., the disk resonator is relatively thin. However, such agreement cannot be obtained for a thick structure as is shown in Fig. 3. On the other hand, the Hankel transform domain method is believed to be valid even for thicker cases.

*2) Transmission and Reflection Characteristics of the Circular Disk Resonator:* Next, the characteristics of the circular disk resonator filter were investigated experimentally and theoretically. From the traveling wave filter theory [4], the following approximate formula can be derived:

$$|S_{21}|_{\min} = |T - T_0|/|1 - TT_0| \tag{43}$$

$$Q_L = \pi\sqrt{(1+T^2T_0^2)/2}\,/(1-TT_0) \tag{44}$$

$$Q_0 = \pi/(-\ln T_0) \tag{45}$$

where $T_0 = \exp(-\alpha l)$ and $Q_L$, $Q_0$, $T$, and $\alpha$ are the loaded $Q$ factor, the unloaded $Q$ factor, the transmission coefficient of coupled section, and the attenuation coefficient of the ring or disk resonator, respectively. If $|S_{21}|_{\min}$ and $Q_L$

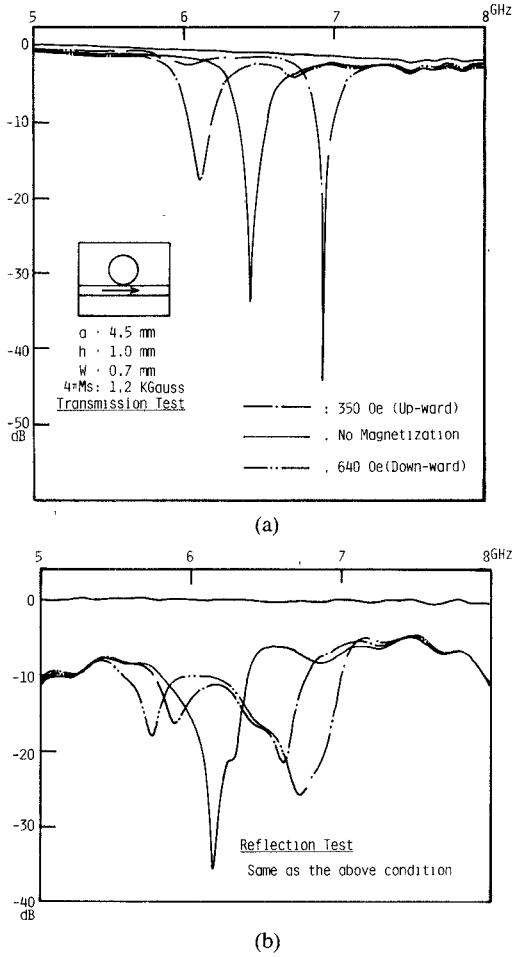


Fig. 6. Measured transmission and reflection coefficients for the circular disk resonator filter on a ferrite substrate.

TABLE I
$Q$ FACTORS AND RELATED QUANTITIES FOR CIRCULAR DISK RESONATOR ON A FERRITE SUBSTRATE

| Hout | res. freq. | BW | $\|S_{12}\|_{\min}$ | $T$ | $T_0$ | $Q_L$ | $Q_0$ | $Q_0$ by f-w a |
|---|---|---|---|---|---|---|---|---|
| 350 Gauss (upward) | 6.11 GHz | 0.30 | -17.0dB | 0.9269 | 0.9240 | 20.37 | 39.73 | 77.0 |
| No Magnetization | 6.44 | 0.26 | -33.5 | 0.9384 | 0.9383 | 24.77 | 49.33 | 128.0 |
| 640 Gauss (downward) | 6.93 | 0.20 | -43.0 | 0.9556 | 0.9556 | 34.65 | 69.20 | 141.0 |

*f-w a: full-wave analysis.

Note: res. freq., $BW$, $|S_{12}|$ min, and $Q_L$ are measured values. $T$, $T_0$, and $Q_0$ are derived from these measured values by (43)–(45).

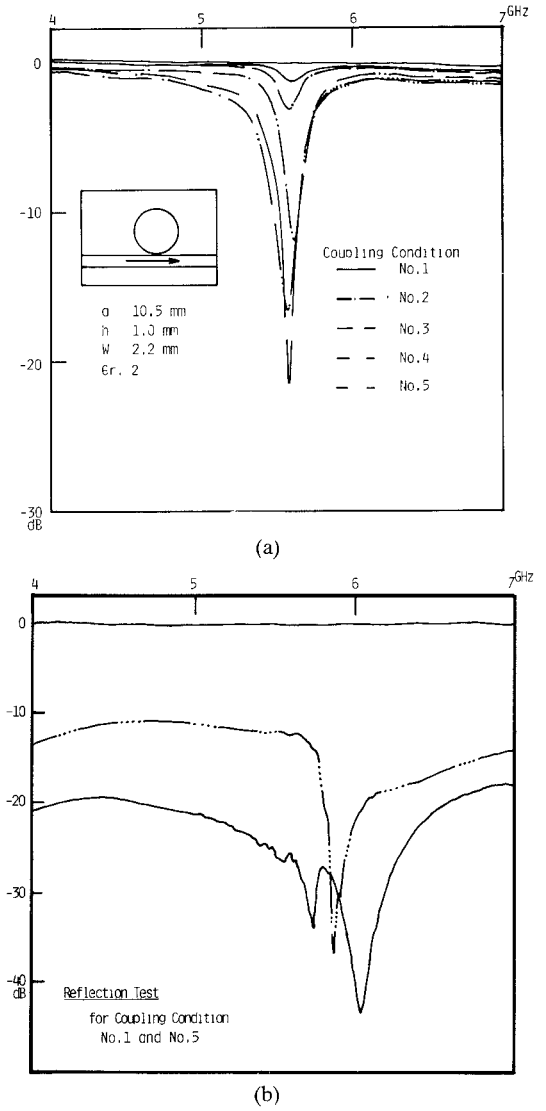


Fig. 7. Measured transmission and reflection coefficients for the circular disk resonator filter on a dielectric substrate.

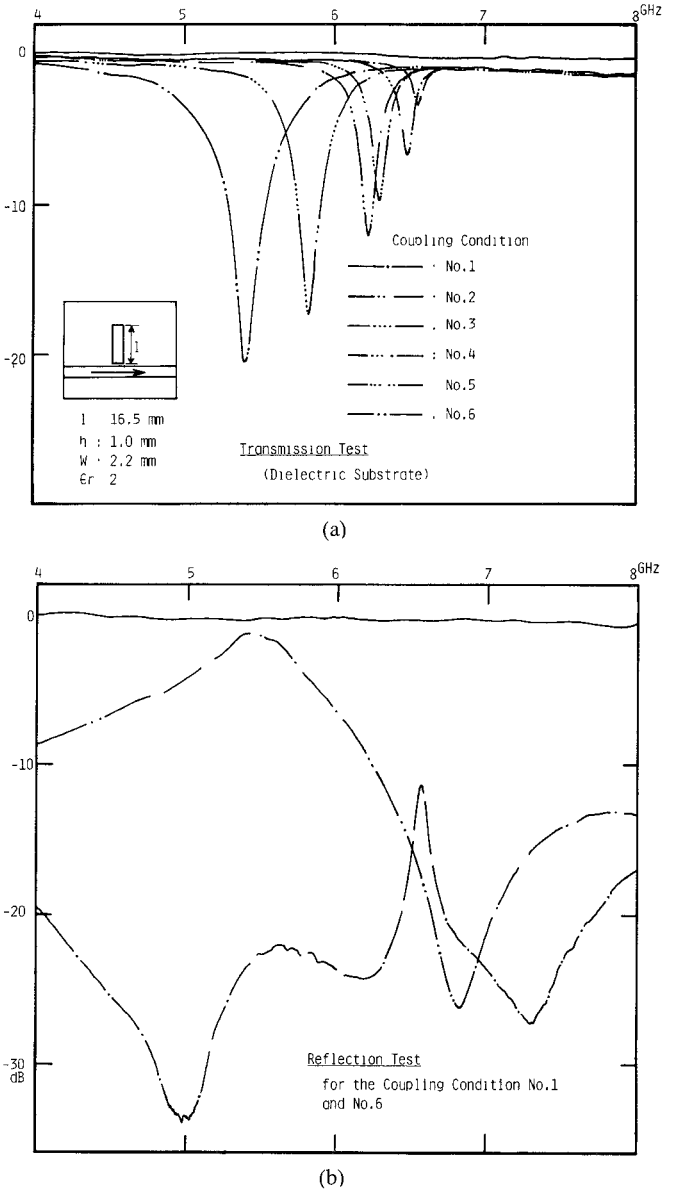


Fig. 8. Measured transmission and reflection coefficients for the standing wave resonant filter on a dielectric substrate.

TABLE II

$Q$ FACTORS AND RELATED QUANTITIES FOR A CIRCULAR DISK RESONATOR ON A DIELECTRIC SUBSTRATE

| coupling condition | res. freq. | BW | $\lvert S_{12}\rvert_{min}$ | T | $T_0$ | $Q_L$ | $Q_0$ | $Q_0$ by f-w a |
|---|---|---|---|---|---|---|---|---|
| No.1 | 5.61 GHz | 0.13 | -1.2dB | 0.9468 | 0.9131 | 31.17 | 36.77 | 47.0 |
| No.2 | 5.59 | 0.13 | -3.0 | 0.9736 | 0.9306 | 31.00 | 43.67 | 47.0 |
| No.3 | 5.61 | 0.24 | -11.6 | 0.9404 | 0.9317 | 23.33 | 44.41 | 47.0 |
| No.4 | 5.57 | 0.37 | -16.4 | 0.9097 | 0.9060 | 15.05 | 31.83 | 47.0 |
| No.5 | 5.58 | 0.32 | -21.2 | 0.9140 | 0.9130 | 17.44 | 34.41 | 47.0 |

*f-w a: full-wave analysis.

Note: res. freq., $BW$, $|S_{12}|$ min, and $Q_L$ are measured values. $T$, $T_0$, and $Q_0$ are derived from these measured values by (43)–(45).

are measured, $Q_0$ can be estimated through the above equations.

Fig. 6 shows the measured transmission and reflection coefficients for the circular disk resonator filter mentioned previously, and Table I depicts the $Q$ factors and related quantities calculated in accordance with (43)–(45). The theoretical $Q_0$'s are also provided by the full-wave analysis in Figs. 3 and 4. Here, theoretical $Q_0$'s are twice or two and a half times as large as those derived from the experiments. This can be explained by the fact that the ferrite material has considerable material loss in the case where it is partially magnetized. It was clearly shown that if the external dc magnetic field applied upward, $Q_0$ is smaller than that of the downward case as shown in Figs. 2, 3, and 4.

Furthermore, a circular disk resonator on a dielectric substrate was measured to confirm the traveling wave filter theory. Fig. 7 shows the measured transmission and reflection coefficients for the resonator on the dielectric substrate ($\epsilon_r = 2$) with a range of coupling conditions, and Table II shows the $Q$ factors calculated by the same

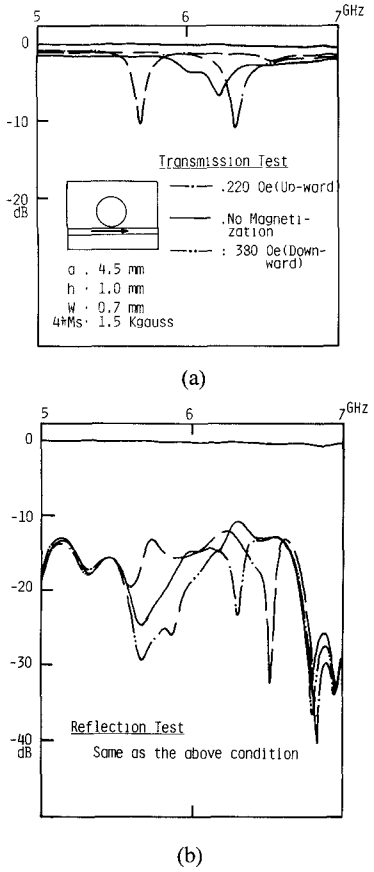


Fig. 9. Measured transmission and reflection coefficients for the circular disk resonator filter on a ferrite substrate.

TABLE III

*Q* FACTORS AND RELATED QUANTITIES FOR A STANDING WAVE RESONATOR ON A DIELECTRIC SUBSTRATE

| coupling condition | res. freq. | BW | $\|S_{12}\|_{min}$ | $Q_L$ | $Q_0$ |
|---|---|---|---|---|---|
| No.1 | 6.45 GHz | 0.09 | -3.2 dB | 71.67 | 103.60 |
| No.2 | 6.48 | 0.13 | -7.1 | 49.85 | 112.88 |
| No.3 | 6.29 | 0.19 | -10.2 | 33.11 | 107.13 |
| No.4 | 6.22 | 0.25 | -12.4 | 24.88 | 103.72 |
| No.5 | 5.82 | 0.34 | -17.6 | 17.18 | 129.85 |
| No.6 | 5.40 | 0.73 | -20.8 | 7.40 | 81.11 |

*$\epsilon_r$ of dielectric substrate: 2.0.

Note: res. freq., *BW*, $|S_{12}|$ min, and $Q_L$ are measured values. $T$, $T_0$, and $Q_0$ are derived from these measured values by (43)–(45).

methods as above. The $Q_0$ by the full-wave analysis is estimated by [3], which also presented Hankel Transform Domain approach of a circular disk conductor printed on a dielectric substrate. As we can see in Table II, the $Q_0$ obtained by the full-wave analysis agrees with the measured data relatively well. It is, therefore, proved that the dielectric materials have very low material losses ($\tan\delta \simeq 10^{-4}$) so that the material losses of dielectric substrates affect the results of $Q_0$ far less than that of the case of ferrite materials. Furthermore, the variations of the loaded $Q, Q_L$, and the reflection level with the coupling strength between external microstrip line and disk resonator are relatively small.

Next, experiments for a standing wave resonator filter on a dielectric substrate are performed so as to compare the characteristics of the two types of resonators. The results obtained are shown in Fig. 8 and Table III, which show clearly that the loaded $Q$ becomes smaller gradually as the coupling increases even though $Q_0$ is almost constant. In addition, the reflection level becomes extremely high in the nearby frequency band as well as at the center of its resonant frequency. The amount of reflection over the whole frequency band is also greater when the coupling is tighter. These characteristics reveal the considerable defects of the standing wave resonator filter. On the other hand, for the circular disk resonator, the reflection level is almost constant or varies only slightly at the resonant frequency or nearby as shown in Figs. 6 and 9. Also, of much importance, the variations of the loaded $Q$ factors with coupling in the circular disk resonator were shown to be small compared with those of a standing wave resonator.

## IV. CONCLUSION

A full-wave analysis of a circular disk printed circuit resonator or antenna on a magnetized ferrite substrate was shown based on the spectral (Hankel transform) domain approach. The method has many attractive features for numerical analysis. Numerical results for the natural resonant frequencies have shown to be in good agreement with experimental data. Although only the dominant mode is studied numerically, the method itself is applicable to higher order modes as well.

Radiation patterns, for which time consuming inverse Hankel transformation is not required, can easily be obtained although they have not been measured and calculated yet. Such work will be carried out in the near future. The advantages of the traveling wave filters over the standing wave filters are demonstrated experimentally and theoretically. Development of the refined design will be planned.

## APPENDIX I

### BASIS FUNCTIONS AND HANKEL TRANSFORMATIONS FOR THE CURRENT DISTRIBUTION

Considering the edge condition [5], we chose the following basis functions:

$$J_{ri}(r) = r^{2(i-1)}(a^2 - r^2)^{1/2} \qquad (i = 1,2,\cdots)$$

$$J_{\phi i}(r) = r^{2(i-1)}(a^2 - r^2)^{-1/2} \qquad (i = 1,2,\cdots).$$

Fortunately, all functions defined above can be analytically Hankel transformed and these Hankel transforms can be expressed in terms of elementary functions in the case of the odd order ($n = 1,3,\cdots$).

The Hankel transformations of the basis functions used for the dominant mode ($n = 1$) are given below.

$$\tilde{J}_{r1}^{+}=\int_0^a J_{r1}J_2(\alpha r)r\,dr=\frac{1}{\alpha^2 a}[2+\cos\alpha a-3\sin\alpha a/\alpha a]$$

$$\tilde{J}_{r1}^{-}=\int_0^a J_{r1}J_0(\alpha r)r\,dr=\frac{1}{\alpha^2 a}[-\cos\alpha a+\sin\alpha a/\alpha a]$$

$$\tilde{J}_{r2}^{+}=\frac{1}{\alpha^2 a}[15\sin\alpha a/\alpha^3a^3-15\cos\alpha a/\alpha^2a^2-6\sin\alpha a/\alpha a+\cos\alpha a]$$

$$\tilde{J}_{r2}^{-}=\frac{1}{\alpha^2 a}[-9\sin\alpha a/\alpha^3a^3+9\cos\alpha a/\alpha^2a^2+4\sin\alpha a/\alpha a-\cos\alpha a]$$

$$\tilde{J}_{\phi1}^{+}=\frac{1}{\alpha^2 a}[\alpha-2\cos\alpha a-\alpha a\sin\alpha a]$$

$$\tilde{J}_{\phi1}^{-}=\sin\alpha a/\alpha$$

$$\tilde{J}_{\phi2}^{+}=\frac{1}{\alpha^2 a}[3\sin\alpha a/\alpha a-\alpha a\sin\alpha a-3\cos\alpha a]$$

$$\tilde{J}_{\phi2}^{-}=\frac{1}{\alpha^2 a}[-\sin\alpha a/\alpha a+\cos\alpha a+\alpha a\sin\alpha a].$$

## Appendix II
## Dispersion Formulas for Tensor Permeability of Magnetized Ferrite

### A. In the Case of Saturation

For a ferrite material magnetized to saturation in the $z$-direction, the microwave permeability is a tensor of the form

$$\vec{\mu}=\begin{bmatrix}\mu & -j\kappa & 0\\ j\kappa & \mu & 0\\ 0 & 0 & \mu_z\end{bmatrix}$$

where

$$\mu=1+\omega_m\omega_i/(-\omega^2+\omega_i^2)$$
$$\kappa=\omega\omega_m/(-\omega^2+\omega_i^2)$$
$$\mu_z=1.$$

### B. In the Case of Partial Magnetization

It is known that the tensor permeability as shown below for the partially magnetized state has proposed as experimental formulas empirically fit to experimental data [6]

$$\kappa=-\omega_0/\omega$$
$$\mu_0=\frac{2}{3}\left[1-(\omega_m/\omega)^2\right]^{1/2}+\frac{1}{3}$$
$$\mu=\mu_0+(1-\mu_0)(\omega_0/\omega_m)^{3/2}$$
$$\mu_z=\mu_0^{(1-\omega_0/\omega_m)^{5/2}}.$$

## Acknowledgment

The authors wish to express their thanks to Prof. T. Itoh of the University of Texas at Austin for many helpful suggestions.

## References

[1] S. Mao, *et al.*, "Millimeter-wave integrated circuits," *IEEE Trans. Microwave Theory Tech.*, vol. MTT-16, pp. 455–461, 1968.
[2] Y. T. Lo, D. Solomon, and W. F. Richard, "Theory and experiment on microstrip antennas," *IEEE Trans. Antennas Propagat.*, vol. AP-27, Mar. 1979.
[3] K. Araki and T. Itoh, "Hankel transform domain analysis of open circular microstrip radiating structures," *IEEE Trans. Antennas Propagat.*, AP-29, Jan. 1981.
[4] G. L. Matthaei, *et al.*, *Microwave Filters, Impedance-Matching Networks, and Coupling Structures.* New York: McGraw-Hill, 1964, ch. 14.
[5] R. Mittra and S. W. Lee, *Analytical Techniques in the Theory of Guided Waves.* New York: Macmillan, 1971, ch.1.
[6] J. J. Green and F. Sandy, "Microwave characterization of partially magnetized ferrite," *IEEE Trans. Microwave Theory Tech.*, vol. MTT-22, pp. 641–651, June 1974.

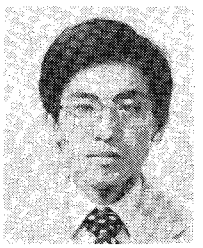

**Kiyomichi Araki** was born in Nagasaki, Japan, on January 7, 1949. He received the B.S. degree in electrical engineering from Saitama University, Urawa, Japan, in 1971, and the M.S. and Ph.D. degrees in physical electronics engineering, both from the Tokyo Institute of Technology, Tokyo, Japan, in 1973 and 1978, respectively.

From 1978 to the present he has been a Research Associate at Tokyo Institute of Technology. From September 1979 to August 1980, he was a Post Doctoral Fellow at the University of Texas, Austin, where he was engaged in the design and development of millimeter wave devices.

Dr. Araki is a member of IECE of Japan.

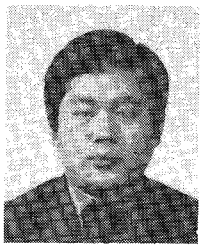

**Dong Il Kim** (S'81) was born in Nonsan, Korea, on February, 26 1952. He received the B.E. and M.E. degrees in nautical science and electronic navigation from the Korea Maritime University, in 1975 and 1977, respectively. Currently he is studying for the Ph.D. degree at the Tokyo Institute of Technology.

He is a Lecturer at Korea Maritime University, and he is currently on leave from Korea Maritime University.

Mr. Kim is a member of the Institute of Electronics and Communication Engineers of Japan and Japan Institute of Navigation.

**Yoshiyuki Naito** (M'70–SM'74) was born in Oita, Japan, on November 22, 1936. He received the B.S. degree in electrical engineering and the D.Eng. degree, from the Tokyo Institute of Technology, Tokyo, Japan, in 1959 and 1964, respectively.

Since 1964 he has been with Tokyo Institute of Technology. From September 1965 to October 1966 he was a Postdoctoral Fellow at Polytechnic Institute of Brooklyn, Brooklyn, NY. Currently, he is a Professor with the Faculty of Engineering. His research has chiefly been concerned with microwave circuit elements, and properties and applications of magnetic material and antennas.

Dr. Naito received an Inada Award in 1961 and a Treatise Award in 1966 from the Institute of Electronics and Communication Engineers of Japan. He is a member of the Institute of Electronics and Communication Engineers of Japan.